Jpn. J. Appl. Phys. Vol. 33 (1994) pp. 6569-6571
Part 1, No. 12A, December 1994

Eye-Safe Compact Mie Scattering Lidar Using a Diode-Laser-Pumped Nd:YAG Laser for Measuring the Atmospheric Boundary Layer

Ichiro MATSUI, Hiroyuki KUBOMURA[1], Hiroshi IMOTO[1] and Nobuo SUGIMOTO
National Institute for Environmental Studies, 16-2 Onogawa, Tsukuba, Ibaraki 305
[1]*NEC Corporation, 1-10 Nisshincho, Fuchu, Tokyo 183*

(Received May 30, 1994; accepted for publication October 15, 1994)

An eye-safe compact Mie scattering lidar for atmospheric boundary layer measurement was developed. The lidar employs a low-pulse-energy high-repetition-rate Q-switched Nd:YAG laser pumped by cw diode lasers. The vertical profiles of aerosols measured with the lidar were found to have sufficient signal-to-noise ratio for observing the structure of the atmospheric boundary layer which plays an important role in air pollution phenomena.

KEYWORDS: lidar, Mie scattering, remote sensing, air pollution, diode-laser-pumped solid-state laser

1. Introduction

The Mie scattering lidar is an effective tool for measuring atmospheric boundary layer structure which is of essential importance in the analysis of air pollution phenomena. Because the density of aerosols is high in the atmospheric boundary layer, the structure of the boundary layer can be visualized by measuring the aerosol density profiles with Mie scattering lidar. Many previous studies have been performed on boundary layer measurement with scanning lidar[1-3] and vertically directed lidar.[4,5] We consider, from the results of these studies, that a network of vertically directed compact Mie scattering lidar devices is of practical use for monitoring and predicting urban air pollution. In this paper, we report on an experiment on an eye-safe and maintenance-free compact lidar for such a purpose.

There are two approaches to meeting the eye-safe criterion which is defined by ANSI Z136.1 (American National Standards Institute)[6] and JIS C 6802 (Japanese Industrial Standards).[7] One is the use of so-called eye-safe lasers which have wavelengths longer than 1.5 μm,[8] and the other is the use of lasers with small output pulse energy. The second approach has been selected in this work. It has been discussed in our previous paper that the eye-safe criterion can be satisfied in a lidar system with a low-pulse-energy high-repetition laser if the output beam is expanded and is shut off immediately when strong return from an obstacle is detected in the lidar signal.[9] The maximum permissible exposure at 1.06 μm is 5×10^{-2} J/m^2, and it approximately corresponds to 390 μJ when the output beam is expanded to 10 cm in diameter. The measurement can be resumed after an intermission of more than 1 s.

The low-pulse-energy approach in our method is similar to that in the micropulse lidar reported by Spinhirne.[10] However, a safety device is adopted in our method, and therefore the reduction factor for the maximum permissible exposure (MPE) for repetitive pulses is not required.[9] This reduction factor is approximately 89 when the repetition rate is 8 kHz, and consequently, the laser pulse with 89 times the energy can be used in our method, in this example.

We have built a compact Mie scattering lidar using a low-pulse-energy diode-laser-pumped Nd:YAG laser, and we have investigated the performance of the system by measuring atmospheric backscattering signals.

2. Experimental

A block diagram of the lidar system is shown in Fig. 1. The parameters of the system are listed in Table I.

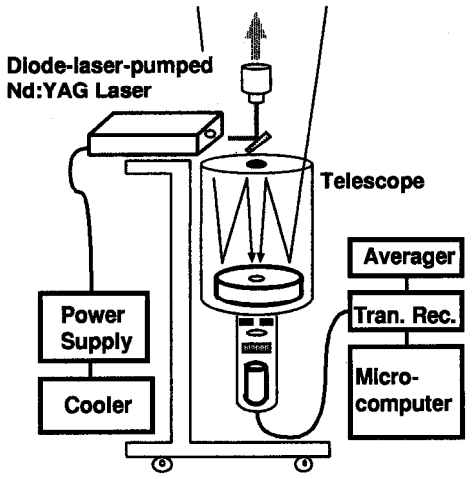

Fig. 1. Block diagram of the lidar system.

Table I. Specifications of the lidar system.

Transmitter	
Diode-laser-pumped Q-switched Nd:YAG laser	
Wavelength	1.06 μm
Pulse repetition	1–8 kHz
Pulse energy	250 μJ at 1 kHz repetition
	100 μJ at 8 kHz repetition
Pulse width	40 ns at 1 kHz repetition
	90 ns at 8 kHz repetition
Receiver	
Cassegrainian telescope	
diameter	35 cm
Detector	
Photomultiplier	
quantum efficiency	0.0005
Data acquisition system	
Transient digitizer	
Sample rate	20 MHz
Accuracy	10 bits
Maximum repetition	500 Hz

The laser is a Q-switched Nd:YAG laser pumped by cw diode lasers. The output pulse energy is 100–250 μJ depending on the repetition rate.

The structure of the laser oscillator is illustrated in Fig. 2. The dimension of the Nd:YAG rod is 1.5 mm in diameter and 12 mm in length. The rod is pumped from the side with two arrays of cw diode lasers from two directions. The angle between the pump directions is approximately 120°. The acoustooptic Q-switch is used to generate pulsed output. The alignment of the laser cavity is adjusted with a pair of wedge prisms located in the oscillator.

Figure 3 shows the characteristics of laser output. The peak power of laser output decreases as a function of the repetition rate, but the averaged output power increases up to 8 kHz repetition. The pulse width is also a function of the repetition rate.

The lidar return signal is collected with a 35-cm-diameter telescope and detected with a photomultiplier tube. The detected signal is recorded with a computer-controlled transient digitizer with a high-speed averager.

The profiles of aerosols in the atmospheric boundary layer were measured with the system. The lidar signal can be expressed as a function of range, R, by the following lidar equation:

$$P(R)=c\beta(R)\exp\left[-2\int_0^R \alpha(r)\,dr\right]\Big/R^2, \qquad (1)$$

where we defined $P(R)$ as the signal measured with the lidar system. Coefficient c is a system constant which includes the quantum efficiency of the detector. β and α represent backscattering and extinction coefficients, respectively. The distribution of aerosol was obtained from the range-corrected signal, i.e., $R^2\times P(R)$. In the following discussion, we also treat a signal which is averaged with the averager as $P(R)$. The signal-to-noise ratio (SNR) of the measured profile is defined by

$$\mathrm{SNR}=P(R)/\sigma[P(R)], \qquad (2)$$

where $\sigma[P(R)]$ represents the standard deviation of $P(R)$.

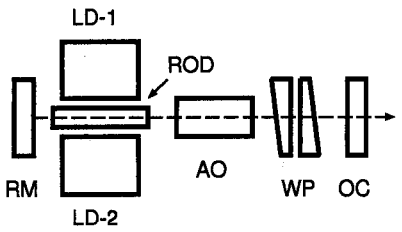

Fig. 2. Structure of the diode-laser-pumped Nd:YAG laser. LD-1, LD-2: diode laser arrays, RM: rear mirror, ROD: Nd:YAG rod, AO: acoustooptic Q-switch, WP: wedge prisms, OC: output coupler.

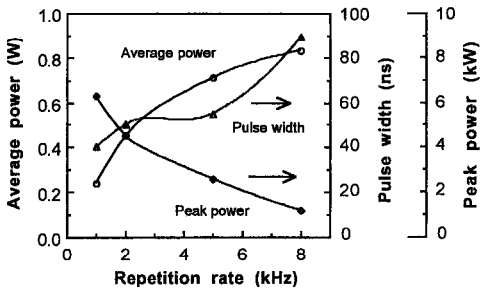

Fig. 3. Characteristics of the diode-laser-pumped Nd:YAG laser. Average power, pulse width and peak power as a function of repetition rate.

3. Results and Discussion

Figure 4(a) shows the lidar return signal as a function of height. The lidar return signals were averaged 4096 times with the averager, and the averaged profile was transferred to the computer. The aerosol profiles up to 1.5 km were measured as seen in Fig. 4(a). The peak at 1.5 km is the strong return from a cloud. Figure 4(b) shows the range-corrected return signal which is approximately proportional to aerosol density. The profiles shown in Figs. 4(a) and 4(b) are the averages of 100 profiles. The standard deviations of the profiles are also indicated in Figs. 4(a) and 4(b). Figure 4(c) shows the SNR of the received signal.

The lidar signal was taken at a rate of 500 Hz, which is the maximum rate of the present data acquisition system, though the laser was operated at 1 kHz. Consequently, it took 8.2 s to measure a single profile, and 13.7 min to measure 100 profiles. The SNR shown in Fig. 4(c) is for a single profile. The SNR for the averaged profile is 10 times higher than that in Fig. 4(c).

We have investigated the characteristics of noise in the measured signals. Figure 5 shows the variance of $P(R)$, $\sigma^2[P(R)]$, as a function of $P(R)$. We can classify different types of noise based on the dependence of $\sigma^2[P(R)]$ on $P(R)$. Background noise, for example, is independent of $P(R)$, and shot noise is proportional to $P(R)$. It can be seen in Fig. 5 that the noise which is in-

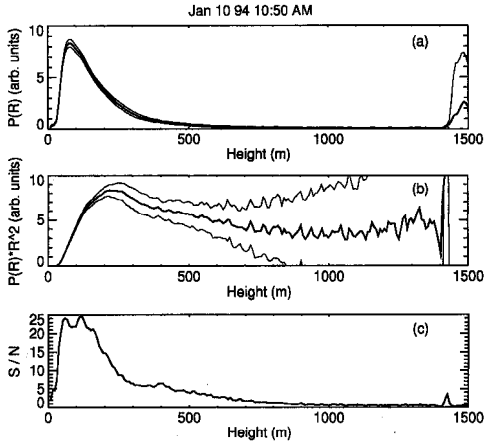

Fig. 4. Atmospheric backscattering signal measured by the lidar as a function of height: (a) intensity of the received signal, (b) the range-corrected signal and (c) the signal-to-noise ratio of the received signal.

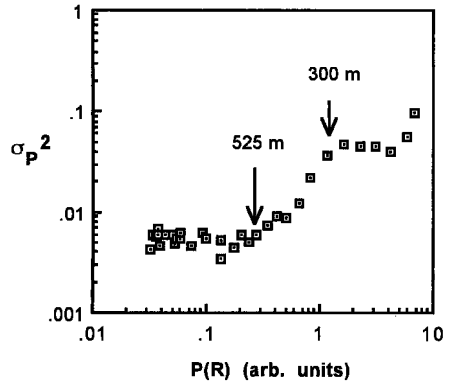

Fig. 5. Variance of the received signal intensity as a function of the received signal intensity.

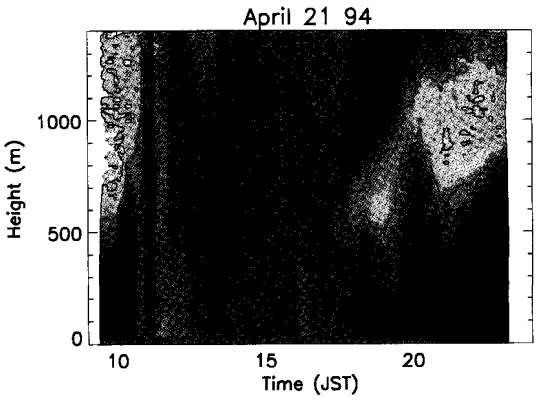

Fig. 6. Diurnal variation of vertical distribution of aerosols observed by the lidar.

dependent on the signal intensity is dominant at height higher than 500 m where $P(R)$ is small. The dominant noise in this region is probably electrical noise, such as amplifier noise, because the background noise due to the solar radiation is considered sufficiently small under the experimental condition. A peak of $\sigma^2[P(R)]$ can be seen in Fig. 5 at the signal intensity corresponding to a height of 300 m. The large variance at this height is probably due to the change in the aerosol profile itself, because this height corresponds to the top of the atmospheric mixed layer.

To demonstrate the performance of the lidar system, we have observed diurnal variation of the aerosol profile with the system. The variation of the range-corrected signal is shown in Fig. 6 as a gray scale and a superimposed contour map. The change in the structure of the boundary layer is clearly seen. This result shows the feasibility of the low-pulse-energy approach in atmospheric boundary layer measurements.

It can be concluded from the analysis of noise in Fig. 5 that the SNR in the present system is limited by the detection system. The SNR of the system can be improved. The use of the photon counting method is considered effective to reduce electrical noise. Also, the use of an avalanche photodiode can improve the SNR because the quantum efficiency at 1.06 μm is much higher than that of the photomultiplier used in the present system.

Also, the SNR of the measurement can be improved if the data acquisition system can operate at 8 kHz repetition instead of the 500 Hz in the present system. The number of lidar returns accumulated in the same measurement time is increased by a factor of 16, though the output pulse energy of the laser at 8 kHz is 0.4 times that at 1 kHz. Consequently, the SNR will increase by a factor of $(16 \times 0.4)^{1/2}$ with this improvement.

We plan to optimize the detection and data acquisition systems and to apply the lidar system to field observations.

1) Y. Sasano, H. Shimizu and N. Takeuchi: Appl. Opt. **21** (1982) 3166.
2) H. Nakane and Y. Sasano: J. Meteorol. Soc. Jpn. **64** (1986) 787.
3) J. L. Schols and E. W. Eloranta: J. Geophys. Res. **97** (1992) 18395.
4) Y. Sasano, H. Shimizu, N. Sugimoto, I. Matsui, N. Takeuchi and M. Okuda: J. Meteorol. Soc. Jpn. **58** (1980) 143.
5) I. Matsui and Y. Sasano: Environ. Sci. **4** (1991) 33.
6) American National Standards Institute: ANSI Standard Z136.1-1986 (1986).
7) Japanese Industrial Standards Committee: JIS C 6802-1991 (1991).
8) N. Sugimoto, N. Sims, K. P. Chan and D. K. Killinger: Opt. Lett. **15** (1990) 302.
9) N. Sugimoto and I. Matsui: Jpn. J. Opt. **21** (1992) 346.
10) J. D. Spinhirne: IEEE Trans. Geosc. Rem. Sens. **31** (1993) 48.